The Astrophysical Journal Letters, 911:L5 (6pp), 2021 April 10 https://doi.org/10.3847/2041-8213/abf14b

^{22}Ne Phase Separation as a Solution to the Ultramassive White Dwarf Cooling Anomaly

Simon Blouin, Jérôme Daligault, and Didier Saumon
Los Alamos National Laboratory, P.O. Box 1663, Los Alamos, NM 87545, USA; sblouin@lanl.gov
Received 2021 March 12; revised 2021 March 22; accepted 2021 March 23; published 2021 April 13

Abstract

The precise astrometric measurements of the Gaia Data Release 2 have opened the door to detailed tests of the predictions of white dwarf cooling models. Significant discrepancies between theory and observations have been identified, the most striking affecting ultramassive white dwarfs. Cheng et al. found that a small fraction of white dwarfs on the so-called Q branch must experience an extra cooling delay of ∼8 Gyr not predicted by current models. ^{22}Ne phase separation in a crystallizing C/O white dwarf can lead to a distillation process that efficiently transports ^{22}Ne toward its center, thereby releasing a considerable amount of gravitational energy. Using state-of-the-art Monte Carlo simulations, we show that this mechanism can largely resolve the ultramassive cooling anomaly if the delayed population consists of white dwarfs with moderately above-average ^{22}Ne abundances. We also argue that ^{22}Ne phase separation can account for the smaller cooling delay currently missing for models of white dwarfs with more standard compositions.

Unified Astronomy Thesaurus concepts: Cosmochronology (332); Degenerate matter (367); Plasma physics (2089); Stellar evolution (1599); Stellar interiors (1606); White dwarf stars (1799)

1. Introduction

White dwarf evolution is often depicted as a simple, uneventful cooling process, implying that they naturally lead to accurate age determinations. White dwarfs are indeed very useful cosmic clocks. They have been used to determine the ages of individual stellar populations (Hansen et al. 2007) and to reconstruct the star formation history of the Milky Way (Tremblay et al. 2014; Kilic et al. 2017; Fantin et al. 2019). When paired with a stellar companion, they also become useful benchmarks for harder-to-model objects (e.g., M, L, and T dwarfs, Lam et al. 2020; Meisner et al. 2020). They could even prove useful to track the galactic evolution of lithium (Kaiser et al. 2021).

However, some aspects of white dwarf cooling remain poorly understood, meaning that the theoretical cooling tracks routinely used to infer white dwarf ages may not be as accurate as they ought to be. The existence of those inaccuracies has been clearly demonstrated during the last few years thanks to the Gaia Data Release 2 (Gaia Collaboration et al. 2016, 2018a). Cheng et al. (2019) revealed the most salient example of the shortcomings of current evolution models by showing that some ultramassive white dwarfs ($M_\star \gtrsim 1.05\,M_\odot$) experience an additional cooling delay of ∼8 Gyr compared to theoretical predictions. Those objects are found in a region of the Gaia color–magnitude diagram (CMD) known as the Q branch (Gaia Collaboration et al. 2018b), which corresponds to an overdensity of objects that coincides with the high-mass tail of core crystallization (Tremblay et al. 2019).

White dwarfs experiencing this additional cooling delay most likely have C/O cores, as the C/O crystallization sequence (and not the O/Ne crystallization sequence) is consistent with the location of the observed overdensity in the Gaia CMD (Bauer et al. 2020, Figure 3). In apparent contradiction with this observation, standard single-star evolution models predict the formation of O/Ne cores in ultramassive white dwarfs (Siess 2007), and ultramassive white dwarfs formed from the merger of two C/O white dwarfs are also predicted to have O/Ne cores (Schwab 2021). However, Althaus et al. (2021) recently proposed two single-star evolution scenarios that can lead to the formation of ultramassive C/O white dwarfs.

Assuming a mass fraction of ^{22}Ne $X(^{22}\mathrm{Ne}) = 0.02$,[1] Cheng et al. (2019) note that, if released during crystallization, the gravitational energy of ^{22}Ne stored in ultramassive C/O white dwarfs is sufficient to generate a ∼6–9 Gyr cooling delay. Such a large effect is possible owing to the neutron-rich nature of ^{22}Ne ($A > 2Z$). The most commonly discussed mechanism to release this potential energy is the gravitational settling of ^{22}Ne in the liquid phase (Bildsten & Hall 2001). However, current models predict that simple gravitational settling is not efficient enough to give rise to multi-Gyr cooling delays (e.g., Bauer et al. 2020), in part because crystallization of the C/O core strongly inhibits the extent of the diffusion of ^{22}Ne in the liquid phase.

Camisassa et al. (2020) proposed that the objects undergoing this extra delay are extremely rich in ^{22}Ne, with a ^{22}Ne mass fraction $X(^{22}\mathrm{Ne}) = 0.06$ instead of the $X(^{22}\mathrm{Ne}) = 0.014$ value expected for white dwarfs issued from the single-star evolution of solar-metallicity progenitors (Cheng et al. 2019). While quadrupling $X(^{22}\mathrm{Ne})$ can indeed produce a multi-gigayear cooling delay, more work is needed to explain how ultramassive white dwarfs could acquire such a high ^{22}Ne abundance. Simulations by Staff et al. (2012) show that mergers of He and C/O white dwarfs can lead to a sizeable ^{22}Ne enrichment. Yet, the stars produced in those merger simulations had a mass of only $0.9\,M_\odot$, meaning that those results may not be directly applicable to ultramassive white dwarfs. Another avenue, explored by Bauer et al. (2020), is to increase the rate of ^{22}Ne gravitational settling through the formation of solid clusters containing a few thousand ^{22}Ne ions. However, subsequent molecular dynamics simulations have shown that the formation of such clusters cannot take place at the low $X(^{22}\mathrm{Ne})$ found in C/O white dwarfs (Caplan et al. 2020). Other avenues unrelated to ^{22}Ne sedimentation

[1] We use X for mass fractions and x for number fractions.

have also been explored, but cannot explain the missing multi-gigayear delay (Horowitz 2020).

In this Letter, we accurately calculate the melting curve of C/O/Ne mixtures to show that the gravitational energy of ^{22}Ne stored in ultramassive white dwarfs can be efficiently released through a phase separation process. Assuming a modest ^{22}Ne enrichment (half of that assumed by Camisassa et al. 2020), this mechanism leads to multi-gigayear cooling delays that can largely explain the ultramassive white dwarf cooling anomaly. We also argue that this process can solve a separate, smaller cooling delay problem that affects standard-composition white dwarfs.

2. The Phase Separation of Neon–22

The possibility of ^{22}Ne phase separation[2] and its effects on the cooling of C/O white dwarfs were first discussed by Isern et al. (1991). The general idea is that depending on the composition of the C/O/Ne plasma and the exact shape of the C/O/Ne phase diagram, the solid crystals that are formed when the crystallization temperature is reached can be depleted in ^{22}Ne with respect to the liquid mixture. If the ^{22}Ne depletion is large enough, those crystals are lighter than the surrounding liquid and float upward, away from the crystallization front. The rising crystals eventually melt in lower density regions where their constituent ions are mixed via Rayleigh–Taylor instabilities. This is analogous to a distillation[3] process and it gradually displaces ^{22}Ne-rich liquid downward. The ^{22}Ne abundance in the liquid at the liquid–solid interface thereby increases until it reaches a critical value for which the C/O/Ne phase diagram predicts that there is no more phase separation (i.e., when the liquidus and solidus meet). The plasma then freezes at this constant composition, forming solid ^{22}Ne-rich layers. The crystallization of the remaining liquid C/O mixture (now free of ^{22}Ne) then continues as usual.

The amount of gravitational energy released in this process critically depends on the exact shape of the C/O/Ne phase diagram. If the distillation process starts immediately at the beginning of the crystallization of the C/O core (i.e., when the core is still fully liquid), then a very large cooling delay is possible. In this scenario, favored by the exploratory calculations of Isern et al. (1991) and Segretain et al. (1994), all the ^{22}Ne from the liquid core is transported to the center of the white dwarf where it forms a compact ^{22}Ne-rich central core. It is also possible, as suggested by the C/O/Ne phase diagram of Segretain (1996), that the distillation process only starts later, when a fraction of the core is already solidified. A ^{22}Ne-rich shell is then formed around a central core with a nearly unperturbed ^{22}Ne concentration. In this scenario, a smaller amount of ^{22}Ne is transported downward and not as deep in the gravitational well of the star, with a more modest energy release.

Caplan et al. (2020) recently used the semianalytic approach of Medin & Cumming (2010) to map the C/O/Ne phase diagram.[4] While they do not discuss this possibility, we note that their Figure 4 confirms that the solid phase can be depleted in ^{22}Ne when the ^{22}Ne concentration remains small in the liquid phase, enabling the distillation process described above. We also remark that their phase diagram indicates that ^{22}Ne distillation will continue (the ^{22}Ne concentration in the liquid will remain higher than that in the solid, $x_{\rm Ne}^{\ell} > x_{\rm Ne}^{s}$)[5] until ($x_{\rm C}$, $x_{\rm O}$, $x_{\rm Ne}$) $\simeq$ (0.8, 0.0, 0.2). This composition corresponds to where the liquidus and solidus meet in the two-component C/Ne phase diagram (see also Figure 4 of Medin & Cumming 2010 and Figure 5 of Ogata et al. 1993).

While past calculations of the C/O/Ne phase diagram support the existence of ^{22}Ne distillation, they are not precise enough to allow an accurate quantitative assessment of the impact of this process on white dwarf cooling. In particular, a high-resolution version of the C/O/Ne phase diagram at small ^{22}Ne concentrations is required. The exact shape of the phase diagram in this region is critical, as it dictates even the qualitative outcome of the distillation process (the formation of a ^{22}Ne-rich central core versus a ^{22}Ne-rich shell closer to the surface).

3. Monte Carlo Simulations

To obtain a high-resolution, high-precision version of the C/O/Ne phase diagram at small ^{22}Ne concentrations, we turn to the Clapeyron integration technique that we have recently developed to map the phase diagrams of dense plasmas (Blouin & Daligault 2021) and applied to the two-component C/O plasma (Blouin et al. 2020). Briefly, this method consists of directly integrating the liquid–solid coexistence line using the appropriate Clapeyron equation for phase transitions at constant temperature and pressure (here, Equation (A2) of Blouin & Daligault 2021), which we evaluate using Monte Carlo simulations where the full electron–ion plasma is considered. All our simulations use $N = 686$ ions, which is enough to mitigate finite-size effects even at very small concentrations ($x_{\rm Ne} \sim 0.002$). We verified this point by performing simulations with up to $N = 4000$ ions. Each simulation is executed for 7×10^6 Monte Carlo iterations, of which the last 5×10^6 are used to evaluate the average thermodynamics quantities needed to integrate the Clapeyron equation. We assume a fixed $P = 10^{24}$ dyn cm^{-2} pressure, a typical value for white dwarf cores. We integrate the melting line at constant temperature T, meaning that many distinct integrations are needed to fully map the C/O/Ne phase diagram in the three-dimensional composition–temperature space (we use 11 different temperatures). It is useful to express the temperature as

$$\Gamma_{\rm C} = \frac{e^2}{a_e k_B T} Z_{\rm C}^{5/3}, \quad (1)$$

where e is the elementary charge, $a_e = (3/4\pi n_e)^{1/3}$ with n_e the electron density, k_B is Boltzmann's constant, and $Z_{\rm C} = 6$. At constant P, n_e is essentially constant in dense degenerate plasmas and $\Gamma_{\rm C}$ is therefore a useful dimensionless measure of T. For reference, a pure C plasma solidifies at $\Gamma_{\rm C} \simeq 175$. The 11 temperatures we simulate are equivalent to $\Gamma_{\rm C}$ ranging from 132 to 182. Those values in turn correspond to the melting

[2] By "^{22}Ne phase separation" we mean the fractionation of ^{22}Ne, whereby the ^{22}Ne concentrations in the coexisting liquid and solid phases differ.

[3] "Creaming" may be a better term to describe this process, but we use "distillation" to remain consistent with previous work on this topic.

[4] Hughto et al. (2012) also studied the liquid–solid coexistence of C/O/Ne mixtures using two-phase molecular dynamics simulations. However, only a handful of compositions were simulated, so that not much can be said about the phase separation of ^{22}Ne from their results.

[5] The solid must be less dense than the liquid for distillation to take place, which is almost (but not rigorously, see Section 3) equivalent to the $x_{\rm Ne}^{\ell} > x_{\rm Ne}^{s}$ condition.

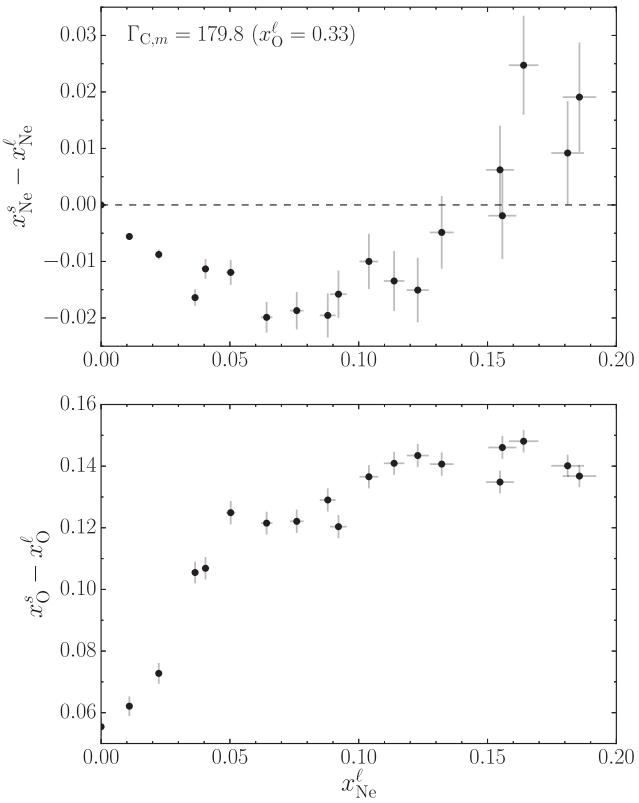

Figure 1. Ne and O concentration changes at the liquid–solid phase transition as a function of the Ne concentration in the liquid phase for a C/O/Ne mixture with $\Gamma_{C,m} = 179.8$. The error bars were obtained by applying the block-averaging technique to our Monte Carlo trajectories and correspond to 1σ confidence intervals. $x_O^\ell = 0.33$ is the O concentration at $x_{Ne}^\ell = 0$ on the coexistence line.

temperatures, $\Gamma_{C,m}$, of C/O plasmas with x_O^ℓ ranging from 0.28 to 0.79.

Figure 1 shows the result of a low-resolution integration of the phase diagram at $\Gamma_C = 179.8$ (the melting temperature of a C/O plasma with $x_O^\ell = 0.33$) between $x_{Ne}^\ell = 0.0$ and $x_{Ne}^\ell = 0.2$. As with the two-component C/O phase diagram, we find that the solid is enriched in O compared to the liquid. As for Ne, the solid can either be enriched or depleted with respect to the liquid depending on the Ne abundance in the liquid. For the temperature used in Figure 1, the solid is depleted in Ne as long as $x_{Ne}^\ell \lesssim 0.15$. It is in this regime that ^{22}Ne distillation is possible.

To precisely determine when the distillation process begins, we performed a set of high-resolution integrations of the phase diagram between $x_{Ne}^\ell = 0.00$ and $x_{Ne}^\ell = 0.05$. For each point along the coexistence line, we evaluate the mass densities ρ of both phases. Figure 2 shows how the solid–liquid density difference varies as a function of x_{Ne}^ℓ for 3 of the 11 temperatures for which we have integrated the C/O/Ne phase diagram. Temperatures and ^{22}Ne concentrations that are below the $\rho^s = \rho^\ell$ line correspond to conditions where ^{22}Ne distillation operates. This regime is reached at low melting temperatures (corresponding to a high $\Gamma_{C,m}$ and a low O concentration) and/or high ^{22}Ne concentrations. Note that even though we found that the solid is always depleted in ^{22}Ne in the $x_{Ne}^\ell \to 0$ limit, its density is not always smaller than that of the liquid as its O enrichment must also be considered.

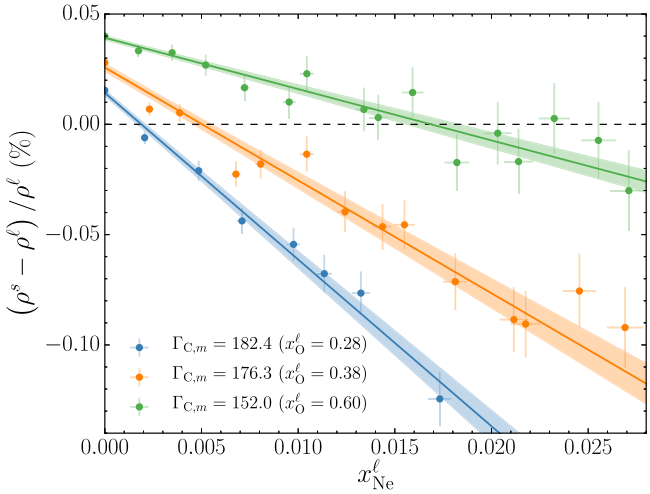

Figure 2. Relative density differences between the liquid and solid phases at the phase transition. The three colors correspond to three different temperatures, as indicated in the legend. As in Figure 1, the x_O^ℓ's correspond to the O concentrations in the liquid phase on the coexistence line at $x_{Ne}^\ell = 0$. The lines are linear fits to our simulation results (shown as circles with error bars) and the shaded regions around them indicate the fit uncertainty.

4. Implications for White Dwarf Cooling

Figure 3 translates the results of Figure 2 in the (Γ_C, x_{Ne}^ℓ) plane for all 11 simulated temperatures. A key finding is that both scenarios described in Section 2 (the formation of a ^{22}Ne-rich central core or shell) are possible depending on the white dwarf's initial composition.

If the central composition of the white dwarf is rich enough in ^{22}Ne (scenario (a) in Figure 3), distillation will start directly at the onset of crystallization when the melting temperature $\Gamma_{C,m}$ is reached in the central layers. The core will remain entirely liquid until the distillation process described in Section 2 increases the ^{22}Ne concentration in the central layers to the critical $x_{Ne} = 0.2$ value (the solid crystals keep floating upward, so no solid core can be formed). This ^{22}Ne enrichment process is symbolized by the blue arrow in Figure 3. The central layers will then freeze at the composition (x_C, x_O, x_{Ne}) = (0.8, 0.0, 0.2), which is reached at $\Gamma_{C,m} = 208$. After that, the crystallization of the remaining C/O core will proceed as usual. This will lead to the formation of a ^{22}Ne-rich C/Ne solid core surrounded by a C/O mantle completely depleted of ^{22}Ne. This final state can also be attained if the central mixture is O poor, in which case the melting temperature is lower and distillation can start right at the beginning of the crystallization process even with a small ^{22}Ne concentration. This corresponds to scenario (b) in Figure 3.

If a more standard composition is assumed (e.g., scenario (c), $X(O) = 0.60$ and $X(^{22}Ne) = 0.014$, or $x_O = 0.53$ and $x_{Ne} = 0.009$), then no ^{22}Ne distillation can initially occur and crystallization takes place as in the case of a two-component C/O plasma without any significant change to the ^{22}Ne distribution. As the crystallization front progresses outward, the liquid is gradually depleted in O due to C/O phase separation and it freezes at increasingly lower temperatures (Horowitz et al. 2010; Althaus et al. 2012; Blouin et al. 2020). Eventually, $\Gamma_{C,m}$ crosses the boundary that delimits the distillation regime and ^{22}Ne distillation can start (this corresponds to the tip of the orange arrow in Figure 3). The progression of the crystallization front is halted until the

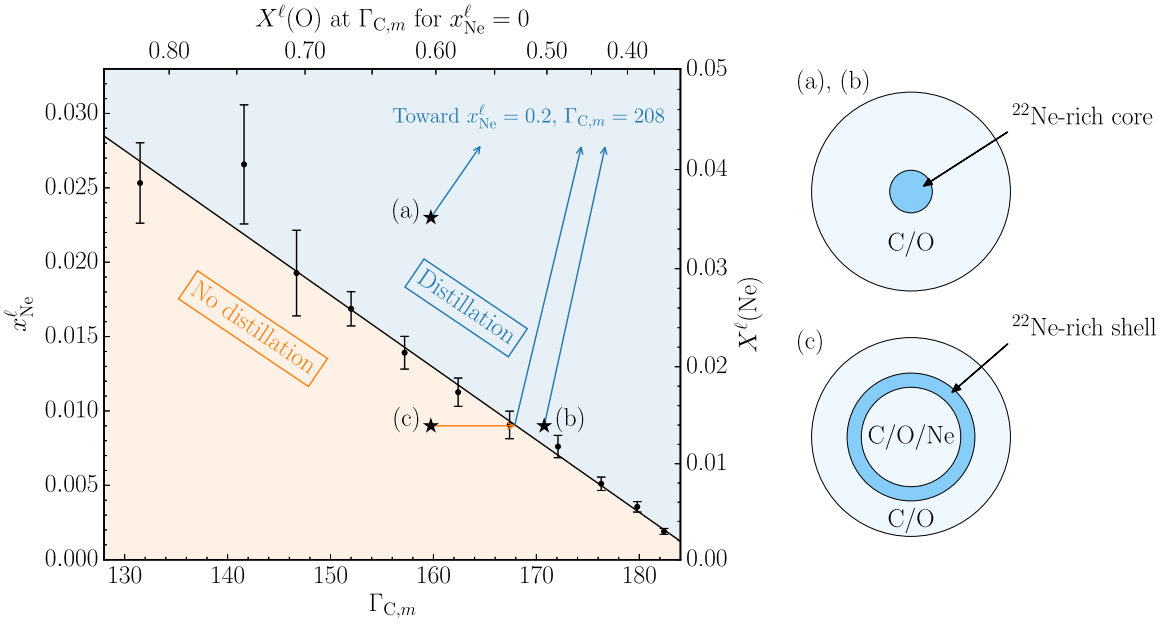

Figure 3. The circles with error bars indicate the conditions where we find that $\rho^s = \rho^\ell$ at the phase transition. The orange region below the line formed by those error bars corresponds to the regime where the solid sinks and no distillation takes place. The blue region corresponds to where the solid is lighter than the liquid, leading to ^{22}Ne distillation. The top horizontal axis gives the O mass fraction in the liquid for a C/O plasma that crystallizes at the temperature given by the bottom axis. The different scenarios (a), (b), and (c) are discussed in the text.

distillation process increases the ^{22}Ne abundance in the liquid at the liquid–solid interface to $x_{Ne} = 0.2$. The ^{22}Ne-rich layers surrounding the solid core then freeze, and the crystallization of the remaining C/O layers continues following the two-component C/O phase diagram. This leads to a final structure where a C/O/Ne central core is surrounded by a ^{22}Ne-rich C/Ne shell, which is itself surrounded by a C/O outer shell completely depleted of ^{22}Ne.

How much does this process affect white dwarf cooling? To answer this question, we generate white dwarf structures using STELUM (Bédard et al. 2020; A. Bédard et al. 2021, in preparation) and compute their binding energies

$$B = -\left(\int_0^{M_\star} u dm - \int_0^{M_\star} G\frac{m}{r} dm\right), \quad (2)$$

where u is the internal energy per unit mass, G is the gravitational constant, and the integrals are performed over the whole star. The net energy released by the distillation process corresponds to the difference in binding energy, ΔB, between the white dwarf structure at the onset of ^{22}Ne phase separation and the structure obtained once it ends.

For the initial structure, we assume that ^{22}Ne is homogeneously mixed throughout the C/O core. This is not strictly correct as ^{22}Ne gravitational settling in the liquid phase will create a ^{22}Ne concentration gradient, but this effect is small (e.g., Figures 2 and 3 of García-Berro et al. 2008) and can be neglected for our purpose. For simplicity, we also assume that the C/O abundance ratio is constant throughout the core. For the final structure, we place all the ^{22}Ne in a central core of mass $M_\star X(^{22}\mathrm{Ne})/X^a(^{22}\mathrm{Ne})$, where $M_\star$ is the white dwarf's mass, $X(^{22}\mathrm{Ne})$ is its overall ^{22}Ne mass fraction, and $X^a(^{22}\mathrm{Ne}) = 0.3$ is the ^{22}Ne mass fraction in the central core (i.e., $x_{Ne} = 0.2$). If a ^{22}Ne-rich shell is formed instead, then its mass is given by $M^\ell_\star X(^{22}\mathrm{Ne})/X^a(^{22}\mathrm{Ne})$, where $M^\ell_\star$ is the mass of the fraction of the core that is still liquid when the distillation process starts. Table 1 gives the resulting ΔB for different scenarios. We also estimate the resulting cooling delay by dividing this ΔB by the average luminosity of the star over the distillation process.[6]

Table 1
Effect of ^{22}Ne Phase Separation

$M_\star$ ($M_\odot$)	X(O)	$X(^{22}\mathrm{Ne})$	log $L/L_\odot$[a]	ΔB (10^{47} erg)	$\Delta\tau$ (Gyr)
Formation of a ^{22}Ne-rich central core					
1.0	0.50	0.035	−3.0	10	9.0
1.0	0.60	0.035	−2.9	10	6.4
1.1	0.50	0.035	−2.8	15	7.1
1.1	0.60	0.035	−2.6	15	5.0
1.2	0.50	0.035	−2.4	23	4.6
1.2	0.60	0.035	−2.3	23	3.6
Formation of a ^{22}Ne-rich shell					
0.6	0.60	0.014	−4.1	0.18	1.8
0.8	0.60	0.014	−3.8	0.34	2.0
1.0	0.60	0.014	−3.5	0.66	1.6

Note.
[a] Average luminosity of the star over the distillation process.

The first portion of Table 1 gives the impact of ^{22}Ne phase separation on ultramassive ^{22}Ne-rich white dwarfs that will form a ^{22}Ne-rich central core as in scenario (a) of Figure 3. For those models, we use the $X(^{22}\mathrm{Ne}) = 0.035$ value discussed in Bauer et al. (2020) for white dwarfs that descend from stars formed in α-rich environments. However, our conclusions are not limited to this particular scenario; any other scenario that leads to a moderate ^{22}Ne enrichment can be envisaged (e.g., the merger of two white dwarfs; Blouin et al. 2020; Camisassa et al. 2020). We find that ^{22}Ne phase separation induces an

[6] A thick $M_H/M_\star = 10^{-4}$ H envelope is assumed in all cases.

additional 4–9 Gyr cooling delay for those objects, which explains most of the ultramassive white dwarf cooling anomaly. An abundance of $X(^{22}\mathrm{Ne}) = 0.035$ is expected to be rare in white dwarfs, which is consistent with the fact that only ∼6% of ultramassive white dwarfs are affected by the cooling anomaly (Cheng et al. 2019). Depending on the mass and composition of the white dwarf, the delay induced by ^{22}Ne phase separation can be short of the 8 Gyr delay inferred by Cheng et al. (2019), but there are additional factors to consider:

1. The ^{22}Ne mass fraction for the delayed ultramassive white dwarfs may well be higher than the $X(^{22}\mathrm{Ne}) = 0.035$ value assumed here.
2. As explained in Bauer et al. (2020), the missing cooling delay can be reduced to ∼6 Gyr by changing some assumptions in Cheng et al.'s analysis, such as the thick disk age, the age–velocity dispersion relation, and the star formation history.
3. The C/O white dwarf cooling tracks used by Cheng et al. (2019) for $M_\star < 1.10\,M_\odot$ do not include C/O phase separation (Fontaine et al. 2001), meaning that they underestimate the time those objects stay on the Q branch by up to ∼1 Gyr (Blouin et al. 2020).
4. Cheng et al. (2019) use O/Ne white dwarf cooling tracks (Camisassa et al. 2019) for $M_\star \geqslant 1.10\,M_\odot$, but it is increasingly clear that the objects that form the delayed population have C/O cores (Bauer et al. 2020; Camisassa et al. 2020). As pointed out by Bauer et al. (2020), O/Ne white dwarfs crystallize much earlier in their evolution than C/O white dwarfs (i.e., at higher luminosities), meaning that the latent heat and gravitational energy released during crystallization induce a shorter cooling delay and that ^{22}Ne diffusion has less time to operate. From Figure 2 of Camisassa et al. (2020), we infer that this led Cheng et al. (2019) to overestimate by ∼1.5 Gyr the cooling delay experienced by $M_\star \geqslant 1.10\,M_\odot$ objects assuming they have C/O cores.

Overall, the cooling delay provided by ^{22}Ne phase separation appears to be the key piece of missing physics required to explain the ultramassive white dwarf cooling anomaly. Note that our results provide further support for the idea that the delayed population identified by Cheng et al. (2019) have C/O cores, as ^{22}Ne distillation cannot take place in O/Ne cores. Neglecting quantum effects in the ionic degrees of freedom, the phase diagram does not discriminate between ^{20}Ne and ^{22}Ne. The total ^{20}Ne+^{22}Ne abundance being higher than that of the azeotrope (Figure 1 of Camisassa et al. 2019), the solid will be enriched in ^{20}Ne and ^{22}Ne, making it denser than the liquid. A sedimentation process analogous to that occurring in C/O white dwarfs will take place.

Any solution to the ultramassive cooling anomaly must also preserve the existing agreement between theory and observations for normal-composition white dwarfs. For instance, the luminosity function of massive white dwarfs in the range of $0.9 < M_\star/M_\odot < 1.1$ is relatively well fitted using current evolution models (Tremblay et al. 2019; Blouin et al. 2020). An additional multi-gigayear cooling delay for those objects can be ruled out. If a standard $X(^{22}\mathrm{Ne}) = 0.014$ abundance is assumed instead of $X(^{22}\mathrm{Ne}) = 0.035$, a ^{22}Ne-rich shell is formed, as in scenario (c) of Figure 3. Much less gravitational energy is then released, which, as needed, leads to shorter cooling delays (Table 1).

Instead of occurring at the onset of crystallization, those delays now occur once ∼60% of the core is already crystallized (assuming an homogeneous $X(\mathrm{O}) = 0.60$ C/O initial profile). Very promisingly, a cooling delay of the order of ∼1 Gyr that manifests itself once ∼60% of the core is crystallized is missing from current C/O cooling tracks (Figure 2 of Blouin et al. 2020 and Figure 19 of Kilic et al. 2020). ^{22}Ne phase separation is very likely the solution to this second problem, although detailed evolutionary calculations that include ^{22}Ne gravitational settling in the liquid phase will be needed to confirm this hypothesis.

Finally, what about ^{22}Ne-rich normal-mass white dwarfs? A $0.6\,M_\odot$ white dwarf with $X(^{22}\mathrm{Ne}) = 0.035$ and $X(\mathrm{O}) = 0.60$ would experience a very long cooling delay of ≈12 Gyr ($\Delta B = 2.1 \times 10^{47}$ erg) during the formation of its ^{22}Ne-rich central core at $\log L/L_\odot \approx -3.9$. However, no discrepancy between the dynamical and photometric ages of the sort discovered for ultramassive white dwarfs (Cheng et al. 2019) has so far been identified for normal-mass objects. If confirmed, this nondetection can be explained in two ways:

1. Very few normal-mass white dwarfs are enriched in ^{22}Ne to the level required to form a ^{22}Ne-rich central core. This would suggest that a negligible number of white dwarfs in the solar neighborhood were formed in α-rich environments, challenging Bauer et al.'s hypothesis that the delayed ultramassive population originates from such environments. In this context, the idea that the delayed ultramassive white dwarfs acquired their high ^{22}Ne content during a merger event (Blouin et al. 2020; Camisassa et al. 2020) may be more promising.
2. Alternatively, the central layers of normal-mass white dwarfs may be much more rich in O than currently assumed (e.g., $X(\mathrm{O}) \simeq 0.85$; Giammichele et al. 2018), which would lead to the formation of a ^{22}Ne-rich shell (Figure 3), with a much smaller cooling delay.

5. Conclusion

We have shown that ultramassive white dwarfs experiencing a long delayed cooling on the Q branch likely correspond to a population of ^{22}Ne-rich C/O white dwarfs in which ^{22}Ne phase separation induces a multi-gigayear cooling delay through the formation of a ^{22}Ne-rich central core. Such multi-gigayear delays are not observed for the vast majority of white dwarfs since, for canonical element abundances, ^{22}Ne phase separation leads instead to the formation of a ^{22}Ne-rich shell closer to the surface. In this case, a smaller cooling delay, which is actually required by current observational data, is generated. The fact that the qualitative outcome of ^{22}Ne phase separation depends on the ^{22}Ne mass fraction is the key attribute that allows this process to cause both small cooling delays at standard ^{22}Ne abundances and very long cooling delays at moderately above-average ^{22}Ne abundances. Detailed cooling sequences and population synthesis simulations will be needed to confirm our conclusions.

Future work should focus on building detailed evolutionary models to study the interplay of C/O phase separation and ^{22}Ne settling in the liquid phase with ^{22}Ne phase separation. The phase separation of ^{56}Fe, another minor species with a potentially large impact on white dwarf cooling (Xu & van Horn 1992), should also be investigated using modern simulation methods. Finally, this work motivates further efforts

to better constrain the still poorly known C/O abundance profiles of white dwarfs (Giammichele et al. 2018), whose shape strongly affects the amount of energy released by ^{22}Ne phase separation.

We are grateful to the anonymous referee for useful comments that have improved the manuscript. S.B. thanks A. Bédard and P. Brassard for useful discussions on the STELUM code. Research presented in this article was supported by the Laboratory Directed Research and Development program of Los Alamos National Laboratory under project number 20190624PRD2. This work was performed under the auspices of the U.S. Department of Energy under Contract No. 89233218CNA000001.

ORCID iDs

Simon Blouin https://orcid.org/0000-0002-9632-1436
Jérôme Daligault https://orcid.org/0000-0002-8844-6124
Didier Saumon https://orcid.org/0000-0001-6800-3505

References

Althaus, L. G., García-Berro, E., Isern, J., Córsico, A. H., & Miller Bertolami, M. M. 2012, A&A, 537, A33
Althaus, L. G., Pons, P. G., Córsico, A. H., et al. 2021, A&A, 646, A30
Bauer, E. B., Schwab, J., Bildsten, L., & Cheng, S. 2020, ApJ, 902, 93
Bédard, A., Bergeron, P., Brassard, P., & Fontaine, G. 2020, ApJ, 901, 93
Bildsten, L., & Hall, D. M. 2001, ApJL, 549, L219
Blouin, S., & Daligault, J. 2021, arXiv:2104.00599
Blouin, S., Daligault, J., Saumon, D., Bédard, A., & Brassard, P. 2020, A&A, 640, L11
Camisassa, M. E., Althaus, L. G., Córsico, A. H., et al. 2019, A&A, 625, A87
Camisassa, M. E., Althaus, L. G., Torres, S., et al. 2020, arXiv:2008.03028
Caplan, M. E., Horowitz, C. J., & Cumming, A. 2020, ApJL, 902, L44
Cheng, S., Cummings, J. D., & Ménard, B. 2019, ApJ, 886, 100
Fantin, N. J., Côté, P., McConnachie, A. W., et al. 2019, ApJ, 887, 148
Fontaine, G., Brassard, P., & Bergeron, P. 2001, PASP, 113, 409
Gaia Collaboration, Babusiaux, C., & van Leeuwen, F. 2018b, A&A, 616, A10
Gaia Collaboration, Brown, A. G. A., Vallenari, A., et al. 2018a, A&A, 616, A1
Gaia Collaboration, Prusti, T., de Bruijne, J. H. J., et al. 2016, A&A, 595, A1
García-Berro, E., Althaus, L. G., Córsico, A. H., & Isern, J. 2008, ApJ, 677, 473
Giammichele, N., Charpinet, S., Fontaine, G., et al. 2018, Natur, 554, 73
Hansen, B. M. S., Anderson, J., Brewer, J., et al. 2007, ApJ, 671, 380
Horowitz, C. J. 2020, PhRvD, 102, 083031
Horowitz, C. J., Schneider, A. S., & Berry, D. K. 2010, PhRvL, 104, 231101
Hughto, J., Horowitz, C. J., Schneider, A. S., et al. 2012, PhRvE, 86, 066413
Isern, J., Hernanz, M., Mochkovitch, R., & Garcia-Berro, E. 1991, A&A, 241, L29
Kaiser, B. C., Clemens, J. C., Blouin, S., et al. 2021, Sci, 371, 168
Kilic, M., Bergeron, P., Kosakowski, A., et al. 2020, ApJ, 898, 84
Kilic, M., Munn, J. A., Harris, H. C., et al. 2017, ApJ, 837, 162
Lam, M. C., Hambly, N. C., Lodieu, N., et al. 2020, MNRAS, 493, 6001
Medin, Z., & Cumming, A. 2010, PhRvE, 81, 036107
Meisner, A. M., Faherty, J. K., Kirkpatrick, J. D., et al. 2020, ApJ, 899, 123
Ogata, S., Iyetomi, H., Ichimaru, S., & van Horn, H. M. 1993, PhRvE, 48, 1344
Schwab, J. 2021, ApJ, 906, 53
Segretain, L. 1996, A&A, 310, 485
Segretain, L., Chabrier, G., Hernanz, M., et al. 1994, ApJ, 434, 641
Siess, L. 2007, A&A, 476, 893
Staff, J. E., Menon, A., Herwig, F., et al. 2012, ApJ, 757, 76
Tremblay, P.-E., Fontaine, G., Fusillo, N. P. G., et al. 2019, Natur, 565, 202
Tremblay, P. E., Kalirai, J. S., Soderblom, D. R., Cignoni, M., & Cummings, J. 2014, ApJ, 791, 92
Xu, Z. W., & van Horn, H. M. 1992, ApJ, 387, 662